Tight-binding model for calcium nanoclusters: Structural, electronic, and dynamical properties

Xiao Dong, Guan Ming Wang, and Estela Blaisten-Barojas*
School of Computational Sciences, George Mason University, Fairfax, Virginia 22030, USA
(Received 15 April 2004; revised manuscript received 6 July 2004; published 10 November 2004)

The tight-binding (TB) Hamiltonian is parametrized for Ca nanoclusters by fitting to the energy surfaces of small clusters and to the total energy and band structure of bulk fcc and bcc calcium calculated within an all-electron density-functional formalism. Clusters of 32 to 84 atoms are optimized using the TB model and a combination of molecular dynamics–simulated annealing and genetic algorithms. At zero temperature, magic numbers are predicted for 34-, 37-, 39-, 45-, 53-, 57- 61-, and 82-atoms clusters, which range from 1 to 2 nm in size. The nanoclusters' positive ions keep the same geometrical structure as their neutral counterparts. Novel structures are obtained for 35-, 38-, 43-, 50-, 58-, 59-, 62-, 63-, and 76–84-atoms nanoclusters. There is an enhanced ratio of surface to bulk atoms in these nanoclusters that favors an expansion of the surface bond lengths. Furthermore, based on TB molecular-dynamics results of the mean-square displacement as a function of temperature, a premelting of the surface occurs around 600 K. The energy gap between occupied and empty states in the valence band is cluster-size-dependent. Large fluctuations of this energy gap indicate that nanoclusters with more than 50 atoms have metallic characteristics. A normal mode vibrational analysis predicts that the structure of the magic number clusters is maintained even at temperatures around 600 K.

DOI: 10.1103/PhysRevB.70.205409 PACS number(s): 61.46.+w, 36.40.Cg, 36.40.Ei, 31.15.Gy

I. INTRODUCTION

Calcium is one of the most abundant elements on earth and is widely used when combined with other elements. Calcium and strontium are soft alkaline-earth metals that display important structural changes under pressure which are not characteristic of other metals.[1] For small calcium clusters of up to 13 atoms, the structure, energetics, and electronic structure were studied within the all-electron density-functional approach.[2] A massive computational effort would be needed to investigate clusters of larger sizes at the same level of calculation. It is therefore important to develop a simplified quantum-mechanical model such as the tight-binding approach that would be well parametrized for clusters containing several tens to hundreds of atoms that reach the nanometer-size regime.

Classical studies to model calcium cluster structures in this size range were carried out based on a parametrization on bulk calcium properties[3] of the Murrell-Mottram two- and three-body potential.[4] For small clusters with fewer than 20 atoms, this potential overestimates the binding energies and does not predict the quantum mechanically optimized structures for several cluster sizes.[2] For larger cluster sizes containing several hundreds of atoms, a growth following a pattern that fills atomic icosahedral shells was predicted based on the relative abundance observed in the mass spectrum of hot calcium clusters.[5] However, the structural, electronic, and thermodynamic properties of calcium clusters containing tens of atoms are not well characterized. More specifically, it would be interesting if the structure of nanoclusters could be identified experimentally in this size range. Calcium is very reactive, and nanocluster surface characterization is important.

The mass spectra of calcium and strontium nanoclusters[6–9] display similar but not identical features. In both spectra, clusters with 34 and 61 atoms are very abundant and can be identified as magic numbers. The strontium mass spectrum shows another magic number at Sr_{82} not observed in the calcium mass spectrum. Indeed, the calcium spectrum shows a not too strong abundance peak at Ca_{80}–Ca_{81}.[7,8] Additionally, the calcium mass spectrum shows large abundance at Ca_{37}. Other not so pronounced abundant clusters sizes are observed at Ca_{43} and Ca_{52}.[8] However, in contemporary experiments of the same group,[7] the latter were not clearly detected. The lack of more recent experimental data under better-controlled experimental conditions is unfortunate. Our recent studies of strontium clusters, based on the second-moment-approximation (SMA) many-body potential, have predicted that at low but finite temperatures, the symmetric structures Sr_{34} D_{5h} and Sr_{61} T_d are magic numbers.[9] Predictions for calcium nanoclusters put forward in this study will be of interest to several experimental groups.

Contrary to our successful parametrization of the SMA many-body potential for strontium clusters,[9] we were unable to effectively carry over an equivalent process in the case of calcium. The SMA many-body potential is a classical representation of the tight-binding approach, and recently we have also produced cluster-based parametrizations of SMA many-body potentials for sodium,[10] potassium, cesium,[11] and rubidium.[12] Our SMA many-body potentials have further been used in a variety of studies. For example, Calvo and Spiegelmann[13] used the sodium SMA many-body potential to study phase transitions in sodium clusters containing several tens of atoms.

The calcium cluster electronic structure is different from strontium retaining peculiar quantum characteristics at much larger sizes. Following a fitting strategy similar to Sr,[9] and generalizing the tight-binding (TB) parametrization of bulk calcium,[1] the objectives of this work are (i) to describe a parametrization strategy of the tight-binding model that contains information on the structure and energy of small clusters, as well as on the energy and band structure of fcc and bcc bulk calcium, and (ii) use the so-fitted TB model to

describe the structural and dynamical properties of calcium nanoclusters. This size regime has not been explored for calcium clusters with a simplified quantum-mechanical description. Indeed, considerable work has been done in the past ten years on the issue of the transferability of TB models. TB models constructed from bulk properties were used to study surfaces, or models from selected lattice symmetries were used to study lattices of different symmetries[14–21] The applicability of sets of TB bulk-determined parameters to the study of atomic clusters has also been explored.[22–28] More recently, Xie and Blackman[29] provided a TB model for rhodium within an orthogonal *spd* basis set, which is transferable from clusters to bulk solid. Calcium is very different from rhodium because of the relatively long-range interatomic forces in the alkaline earths and the extended character of the valence band when compared to transition metals. Our recent TB study of bulk calcium reproduced correctly the metal-nonmetal and fcc-bcc pressure-induced transitions,[1] and thus the application of TB to Ca nanoclusters is promising. For sodium, there has been a simplified TB model[13] with parameters fitted on Na_2 and Na_4 (Ref. 30) but not on bulk properties. This simplified TB model did not include *d* orbitals, and the authors find discrepancies between structures calculated with the SMA model and with their TB model for sizes containing more than 40 Na clusters.

In this paper, we generalize the strategy developed for the parametrization of the SMA many-body potential[9–12] and apply it to the parametrization of the TB Hamiltonian. We adopt the Naval Research Laboratory (NRL)-TB model[14,1] to describe the functional dependence of the on-site and hopping integrals with the local environment. This method is described in Sec. II. With the newly parametrized TB model, properties of Ca nanoclusters are explored such as the energetics, structure, stability, and several electronic and thermodynamic properties. Section III presents the calculation of structures of minimum energy for Ca_{32} through Ca_{65} and Ca_{76} through Ca_{84} obtained by simulated annealing carried out with TB molecular dynamics. Section IV escribes the electronic and vibrational properties of these nanoclusters, and Sec. V gives a description of the clusters' finite-temperature properties, including results on the cluster surface premelting. Section VI ends with a brief summary.

II. THE TIGHT-BINDING PARAMETRIZATION FOR CALCIUM NANOCLUSTERS

The adopted TB model is based on the Slater-Koster (SK) approach[31] in which *s*, *p*, and *d* orbitals span a 9×9 matrix representation of the TB Hamiltonian. The *k*-independent parts of the SK Hamiltonian matrix elements are assumed to be parameters. We used a nonorthogonal basis set of atomic orbitals, therefore the number of SK parameters is 24. These matrix elements are the on-site and hopping integrals, which become environment-dependent. Calcium is an element where *d* orbitals should be included because the conduction band has 30% d character. In this work, we adopt the NRL-TB functions for the dependencies of the matrix elements on the local environment[14] such that O_l, the on-site integrals, and H_m, the hopping integrals and nondiagonal elements of the overlap matrix, are

$$O_l(\rho) = \alpha_l + \beta_l\rho^{2/3} + \gamma_l\rho^{4/3} + \delta_l\rho^2, \tag{1}$$

$$H_m(R) = (a_m + b_m R + c_m R^2)e^{-d_m^2 R}F_c(R), \tag{2}$$

where l and m are indices identifying the four on-site integrals and the 20 different hopping integrals and nondiagonal elements of the overlap matrix, respectively. The quantities α_l, β_l, γ_l, δ_l, a_m, b_m, c_m, and d_m are parameters to be fitted and ρ is the local atomic density around each atom i in the cluster,

$$\rho_i = \sum_{j\neq i} e^{-\lambda^2 r_{ij}}F_c(R_{ij}). \tag{3}$$

Here λ is another parameter to be fitted, and R_{ij} is the interatomic distance between atoms i and j. The cutoff function defining the spatial range of every integral is given by

$$F_c(R) = \left[1 + e^{\tau(R/R_0-1)}\right]^{-1}, \tag{4}$$

where $\tau = 91.71$ and $R_0 = 18.35$ Å, such that 19 shells around every atom are included in bulk fcc calcium. In the case of clusters with about 100 atoms, this cutoff ensures that the range of interatomic forces extends outside the volume of the cluster.

Following this scheme, we fitted the 97 parameters entering in Eqs. (1)–(3) to the energy bands and cohesive energy of bulk fcc and bcc calcium[1] and to 30 points of the energy surfaces of Ca_7 through Ca_{13}.[2] For the bulk energies, we considered Seven fcc structures at lattice constants in the range 8.5–11 a.u. and five bcc structures with lattice constants between 7.2 and 8.4 a.u. For the energy bands of each fcc lattice, 85 *k* points of the irreducible Brillouin zone (IBZ) were used in the fit, whereas only 55 *k* points were used for each bcc structure. The bulk calculations were done in the augmented-plane-wave approximation as described in Ref. 1. For the fit to the energies of clusters, we used data calculated within the all-electron general gradient approximation of density functional as described in Ref. 2. Table I identifies the cluster structures used in the fit (column 2), the number of points of each energy surface used in the fit (column 3), and their *ab initio* binding energies E_N from Ref. 2 (column 4). In this fit, we enhanced the weights of the energies by a factor of 16 and decreased accordingly the weights given to the energy bands. The effect is an overall deterioration of the total energy that resulted in an error over the 12 solid structures of 2 mRy. Table II lists the resulting TB parameters for Ca clusters.

Column 5 in Table I lists the cluster binding energies from the TB model using the parameters of Table II. These energies are calculated at the exact geometry of the *ab initio* results (column 4). These geometries are stable under the TB model, however the TB tends to expand slightly all distances. By an isotropic scaling of the coordinates in each cluster, we determine the scaling factor that yields the minimum binding energy under the same structure. One condition imposed in the parametrization procedure was to accept TB parameters only if the scaling factor was smaller than 1.025 for all the structures used in the fit. This condition is satisfied for the TB parameters reported in Table II, as shown in column 6 of Table I. The TB energy at the minimum of the

TABLE I. Structure and binding energy per atom of Ca_6 to Ca_{13} used in the fit of the TB parameters. Energies are in eV/at.

Size	Symmetry	No. points	$-E_N/N$ Ref. 2	$-E_{\mathrm{TB}}/N$	factor	$-E_{\mathrm{TB}}^{\mathrm{scaled}}/N$	$-E'_{\mathrm{TB}}/N$ Ref. 1
6	C_{2v}	2	0.514	0.346	1.02	0.349	0.065
7	D_{5h}	2	0.623	0.506	1.02	0.511	0.325
8	C_s	3	0.638	0.534	1.02	0.538	0.346
9	C_{2v}	7	0.687	0.627	1.02	0.630	0.454
10	C_{4v}	8	0.752	0.7356	1.01	0.736	0.552
11	D_{4d}	2	0.751	0.756	1.0	0.756	0.571
12	C_1	3	0.756	0.741	1.01	0.742	0.591
13	C_1	5	0.781	0.780	1.0	0.780	0.632

scaled geometries is given in column 7. As a comparison, in column 8 are listed the binding energies that would be obtained if the parameters for bulk calcium of Ref. 1 were to be used. It is clear that use of the bulk calcium parameters would underestimate the binding energy. Reciprocally, we also calculated the energy bands of bulk fcc and bcc calcium with this new set of TB parameters and obtained a reasonable agreement at the equilibrium lattice constant. To check the effectiveness of the fitting strategy, an alternative fit was sought in which the same bulk data were included but the energy points of only Ca_6 to Ca_{10} were included in the fit. This "intermediate" parametrization predicted the binding energy of Ca_{11}, Ca_{12}, and Ca_{13} within 2.2% of the *ab initio* results.

III. STRUCTURE OF Ca NANOCLUSTERS

The structure of minimum-energy cluster isomers containing 32 to 84 atoms was searched using a combination of genetic algorithms (GA) and molecular dynamics simulated annealing. In both cases, the TB model was used to calculate the energies. The GA method was described elsewhere.[9,32] The minimum-energy structures obtained with the GA were further relaxed with molecular dynamics simulated annealing. The tight-binding molecular dynamics (TBMD) implementation of Ref. 33 was used throughout with a time step of 1.5 fs. The annealing was done by heating the cluster structure to about 700 K and further cooling down in a steplike manner to 600 K, 400 K, 300 K, 200 K, 100 K, 50 K, and finally 0.001 K. This process was also performed with a set of other preconditioning structures from our database, as well as from known structures characteristic of several model potentials such as Lennard-Jones,[34] Morse,[35] Sutton-Chen,[36] and SMA many-body.[9]

The TBMD relaxation was carried out for every size between Ca_{32-63} and between Ca_{76-84}. This range of sizes is of special interest because it encompasses 34, 61, and 81–82, which are the magic numbers revealed in the mass spectrum of both calcium and strontium.

Results of the binding energy E_N^{neu} of the most stable neutral clusters as a function of cluster size are reported in Table III along with the point-group symmetry identification of every structure. The binding energy is defined as the total TB energy of a neutral cluster with N atoms referred to the TB energy of N isolated atoms. Additionally, we calculated the binding energy E_N^{ion} of cluster cations as a function of size, and the results are shown in Table III. Figure 1 gives a comparison between the neutral and the ionic binding energies. As a test, for certain sizes, such as 34, 45, 61, and 82, the structure of the singly ionized clusters was relaxed in much the same way as for the neutral clusters. Results of this process gave identical lowest-energy structures to those of the neutral clusters, indicating that the structural distortion produced by the lack of one valence electron is negligible. This nanosize result contrasts with the dramatic change in structure that occurs for small clusters up to Ca_9^+.[38] The binding energy decreases very slowly with cluster size such that for Ca_{80} only 82% of the bulk binding energy of −1.84 eV/at (Ref. 38) is attained. Results for the ionic clusters should be seen as estimates, because the TB parametrization was done on data of neutral clusters and neutral bulk.

The second difference of the cluster total energy is an accepted representation of the relative energetic stability correlated to the abundance in the mass spectrum. Figure 2 gives the stability pattern that illustrates how stable is a cluster with N atoms when compared to clusters with neighboring sizes $N-1$ and $N+1$. The pattern reveals magic numbers at 34, 37, 39, 45, 53, 57, 61, and 82 at zero temperature. These nanoclusters are shown in Fig. 3. Except for Ca_{37}, all are highly symmetric structures. The experimental data[8] display 34, 37, and 61 as clusters with high abundance, and 43, 52, and 81 with substantial abundance. These experiments were performed eight years ago, and the temperature was probably high to give rise to an evaporative ensemble. Except for the first three well defined sizes of 34, 37, and 61, this group contemporarily reported slightly different abundances for the other sizes. For example, Ref. 7 identifies fairly abundant 50-, 55-, and 80-atom clusters. We know now that the magic numbers are temperature-dependent and thus new experiments under controlled temperature conditions are highly desirable.

Several of the lowest-energy cluster geometries obtained from the TBMD relaxation process are known structures obtained with the Morse potential,[35] although in the TB clusters the bond lengths are different and most bond angles present significant distortions. The Ca_{34} D_{5h}, Ca_{61} T_d, and Ca_{82} D_{3d}

TABLE II. TB parameters for Ca clusters: $\lambda = 1.12898$ and 96 parameters.

		On-site parameters		
l	α (Ry)	β (Ry)	γ (Ry)	δ (Ry)
s	0.03492	13.105	−503.61	14380
p	0.10997	42.137	−1617	29059
t_{2g}	0.11962	5.1028	−16.74	−967.57
e_g	0.11962	5.1028	−16.74	−967.57
		Hopping parameters		
	a (Ry)	b (Ry/Bohr)	c (Ry/Bohr^2)	d (Bohr$^{-1/2}$)
$ss\sigma$	60.545	−20.512	−1.2402	1.0838
$sp\sigma$	−5.3874	1.4644	−0.0059395	0.77435
$pp\sigma$	−10.248	0.88798	0.33673	0.84042
$pp\pi$	20718	−1092.6	−370.85	1.3381
$sd\sigma$	1.3395	−0.3815	0.021841	0.56738
$pd\sigma$	9.2605	−1.3287	−0.06913	0.82423
$pd\pi$	0.34302	−0.021421	−0.00060766	0.53523
$dd\sigma$	−39.839	15.541	−1.19	0.94669
$dd\pi$	−2.3471	1.0632	−0.06502	0.77388
$dd\delta$	−1312.7	611.91	−70.353	1.231
		Overlap intergral parameters		
	a (Bohr^{-1})	b (Bohr^{-2})	c (Bohr^{-3})	d (Bohr$^{-1/2}$)
$ss\sigma$	7.1342	−0.74684	0.010581	0.69506
$sp\sigma$	44517	−8648.9	23.36	1.3011
$pp\sigma$	53.697	−25.407	1.7451	0.87173
$pp\pi$	493.28	−23.402	6.3334	1.2046
$sd\sigma$	−170.81	28.573	1.7397	0.97778
$pd\sigma$	−41.726	11.434	−0.67112	0.75944
$pd\pi$	−7.3097	0.11654	−0.11793	0.85148
$dd\sigma$	−4.6777	1.5812	−0.072007	0.67429
$dd\pi$	−54717	18273	−1538	1.2233
$dd\delta$	6.966063×10^5	-2.092363×10^5	16132	1.4303

are close to be polytetrahedral constructions, whereas the icosahedral Ca_{45} I_h is built around the McKay 13-atom icosahedron by decorating its 20 faces with one atom each, and adding 12 atoms radially placed from its 12 vertices. Ca_{46} through Ca_{49} keep the McKay 13-atom icosahedron as their core. No other clusters present this icosahedral inner shell. We found several new structures. Namely, the structures of Ca_{35}, Ca_{38}, Ca_{43}, Ca_{50}, Ca_{58}, Ca_{59}, Ca_{62}, Ca_{63}, and Ca_{76}–Ca_{84} have not been reported for any model potential, nor were they in our database. The corresponding clusters are shown in Fig. 4. Ca_{35} is the structure of Ca_{34} (D_{5h}) in which one face is decorated with an extra atom. Ca_{38} is not the usual structure cut from the fcc lattice characteristic of several model potentials such as the Lennard-Jones potential. Instead, the new structure of Ca_{38} has a lower symmetry of C_{2v}. Ca_{43} has a relaxed structure of the inner shell of Ca_{61} with one missing atom. Ca_{50} presents a combination of fivefold and sixfold motifs. The clusters Ca_{58} and Ca_{59} are incomplete Ca_{61} T_d in which two and three of the most external atoms are missing and a local relaxation has occurred. Ca_{62} and Ca_{63} show the onset of an extra shell of atoms on Ca_{61} T_d. Ca_{76} is still fairly spherical, starting to show an ellipsoidal elongation that improves with size to become very pronounced in Ca_{82} D_{3d}.

In these nanoclusters, the nearest-neighbor distances (bond lengths) display a significant dispersion with a non-Gaussian distribution. The tendency is for the "core" atoms to be shorter than the bonds between the "surface" atoms. To show this bond expansion, we performed the following analysis. A coordination sphere of radius 4.6 Å centered on

TABLE III. Structure and binding energy per atom of neutral and charged Ca clusters. Energies are in eV/at.

N	$-E_N^{\mathrm{neu}}/N$	$-E_N^{\mathrm{ion}}/N$	Sym
32	1.24964	1.27288	C_{2v}
33	1.27341	1.29562	C_{5v}
34	1.28520	1.30697	D_{5h}
35	1.28484	1.30534	C_s
36	1.29839	1.31798	C_s
37	1.31410	1.33327	C_s
38	1.32275	1.34004	C_1
39	1.34037	1.35804	C_{2v}
40	1.33638	1.35162	C_s
41	1.35315	1.36718	C_{2v}
42	1.36689	1.38049	C_{3v}
43	1.3794	1.39209	C_{2v}
44	1.38940	1.40053	C_{5v}
45	1.39721	1.40719	I_h
46	1.38758	1.39841	C_s
47	1.38951	1.40145	C_3
48	1.38949	1.40175	C_{2v}
49	1.38754	1.39991	C_s
50	1.39696	1.40849	C_1
51	1.40858	1.41957	C_2
52	1.41933	1.42990	C_s
53	1.42876	1.43897	D_{6d}
54	1.42485	1.43485	C_s
55	1.42456	1.43457	C_1
56	1.43467	1.44455	C_s
57	1.44661	1.45626	D_{3h}
58	1.43751	1.44697	C_s
59	1.44535	1.45474	C_{2v}
60	1.45572	1.46509	C_s
61	1.46481	1.47414	T_d
62	1.45964	1.46883	C_s
63	1.46205	1.47089	C_s
76	1.50034	1.50661	C_s
77	1.50552	1.51185	C_s
78	1.51107	1.51739	C_1
79	1.51761	1.52376	C_1
80	1.52311	1.52969	C_s
81	1.52949	1.53609	C_s
82	1.53541	1.54180	D_{3d}
83	1.52815	1.53444	C_s
84	1.52732	1.53426	C_1

each atom is defined. Inside each sphere, one identifies the nearest neighbors to the atom located in its center. The center of mass (CM) of atoms inside each sphere is calculated and the distance d_{CM} from this point to the central atom is stored. Atoms with $d_{\mathrm{CM}} > 0.7$ Å are identified as surface atoms and all the rest as core atoms. This analysis distinguishes between core atoms having a complete 12-atom coordination shell from surface atoms characterized by coordination shells containing fewer than 12 atom. Following this accounting criterion, the number of surface atoms in the size range under study follows a power law $1.39 \times N^{0.84\pm0.05}$, with an exponent larger than the characteristic $2/3$ exponent of infinite surfaces. Therefore, the nanocluster surfaces are more populated than in extended materials, and the effect of the core atoms is not strong enough to achieve the bond length contraction expected in extended surfaces.

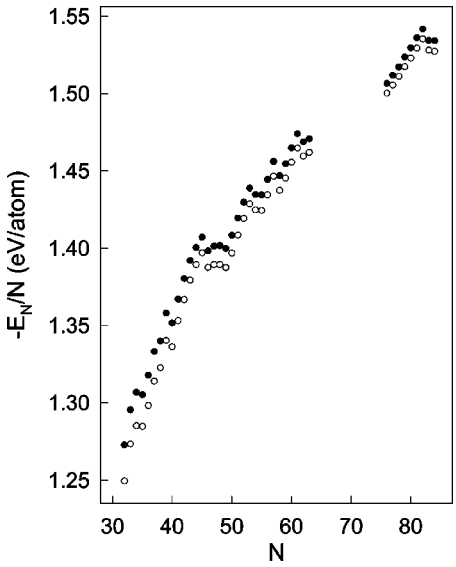

FIG. 1. The binding energy of Ca clusters as a function of cluster size. Empty circles are neutral clusters and black circles are singly ionized positive ions.

Figure 5 shows the results of bond lengths in both core and surface regions. The open circles in this plot are averages of nearest distances between pairs of core atoms and the black circles correspond to nearest distances between pairs of surface atoms. It is very clear that bonds associated to surface atoms are expanded by about 10% for sizes up to about $N=50$ and by about 4% for sizes around $N=80$. This expansion is larger than that obtained with classical model potentials, and it is not related to the spatial frustration that occurs in the McKay icosahedra. For example, the 55-atom McKay icosahedron is a stable isomer of Ca_{55} with energy 1.70 eV above the C_1 structure reported in Table III. In this isomer, the core has 13 atoms and the expansion of the surface bonds

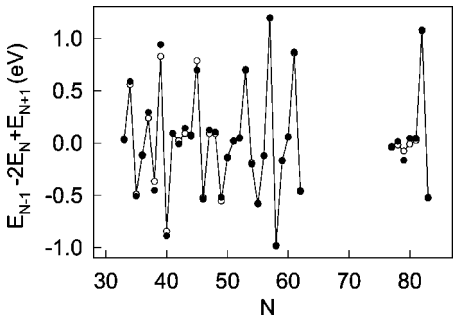

FIG. 2. Second difference of total energy at zero temperature as a function of cluster size.

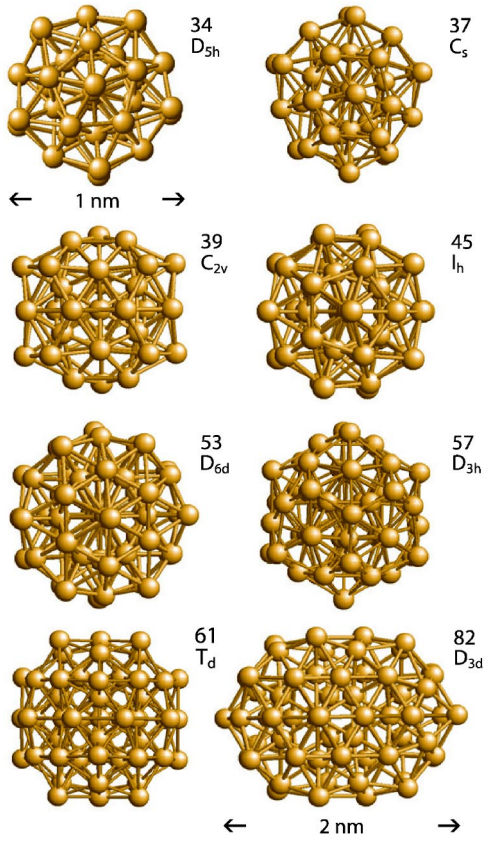

FIG. 3. Structures corresponding to magic numbers of calcium nanoclusters.

with respect to the core bonds is 2%. This contrasts with the 15-atom core and surface bond length expansion of 6% obtained for the TB most stable Ca_{55}. From our results, it is apparent that up to Ca_{49} there is a significant number of fivefold symmetry motifs. However, for larger nanoclusters the hexagonal motifs become more abundant favoring a larger core of atoms with 12-atom coordination shells. In turn, this effect entails rearrangements on the surface such that bonds lengthen in order to generate fairly spherical particles. A general observation is that in the smaller clusters, the surface expansion of amorphouslike higher-energy isomers tends to be smaller than for the ground state. For example, Ca_{34} D_{5h}, Ca_{45} I_h, Ca_{61} T_d, and Ca_{82} D_{3d} present a surface expansion of 8%, 11%, 4%, and 5%, respectively. However, their higher-energy amorphouslike structures display surface expansions of only 3%, 7%, 2% and 5%, respectively.

IV. ELECTRONIC AND VIBRATIONAL PROPERTIES OF THE GROUND STATE

At very low temperature, the Fermi energy is basically constant as a function of the cluster size. The energy gap between the highest occupied valence electron level and the first virtual level is calculated at the equivalent of the IBZ-Γ point for the bulk calcium and displays a size dependence. Figure 6 illustrates the energy gap at zero temperature as a function of cluster size. Values reported in this figure are

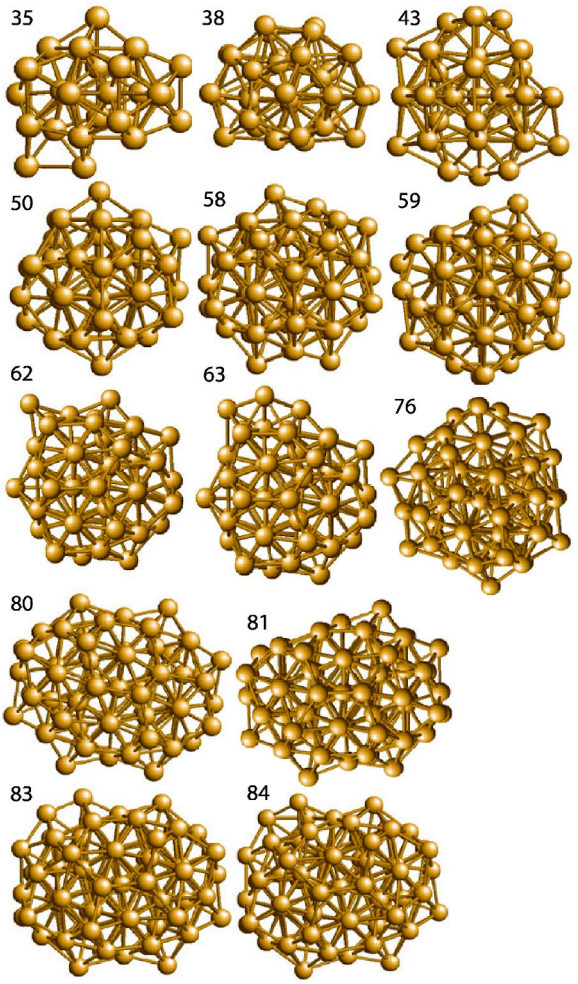

FIG. 4. New calcium nanocluster structures found in this study.

molecular dynamics time averages at 0.001 K. The general trend is a decrease in the average energy gap as the size of the cluster increases. This trend was expected, showing that the metallic character of the nanoclusters is more definite when their size exceeds 49 atoms. Sizes below Ca_{50} tend to have a substantial energy gap, and larger clusters have an incipient metallic character with a low density of states (DOS) at the Fermi energy E_F, as shown in Figs. 7(a) for Ca_{45} and Ca_{45}^+ and in Fig. 7(b) for Ca_{82} and Ca_{82}^+. In this

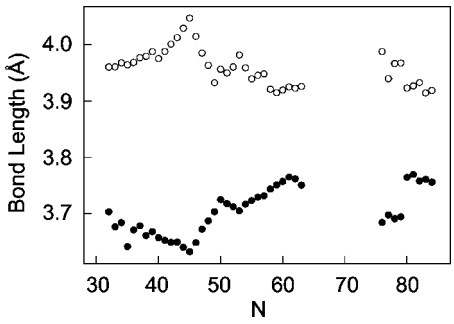

FIG. 5. Bond lengths in the cluster surface (empty circles) and in the cluster inner core (black circles) as a function of size.

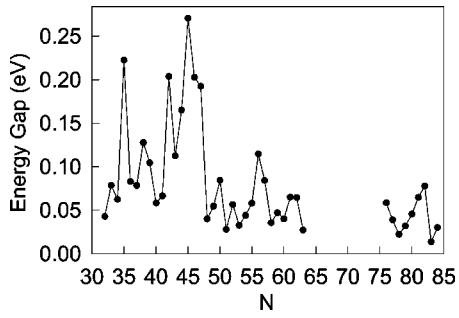

FIG. 6. Energy gap between the occupied and empty states of the valence band as a function of cluster size.

figure, the energy levels are referred to the Fermi energy. The DOS(E_F) in Ca_{45} is clearly zero and in Ca_{82} is still low, approximately 20 times lower than the bulk values.[1] Similar findings were obtained for the cluster ions, as shown in Figs. 7. The peculiar electronic behavior (large energy gaps) for sizes smaller that Ca_{50} might be associated to the large number of fivefold symmetry motifs. This effect was investigated extensively by analyzing the energy gap of 20 higher-energy stable isomers of Ca_{45} available in our database. The large energy gap is observed only in Ca_{45} I_h. In fact, the isomer closest in energy to the icosahedral Ca_{45} is a structure obtained from seeding Ca_{44} with one extra atom. This amorphouslike isomer is 1.4 eV less stable and its energy gap of 0.09 eV is only a third of the icosahedral energy gap. The energy gap of the other 19 isomers of Ca_{45} ranges between 0.02 and 0.06 eV.

Further study of the ground state was achieved through the spectra of normal modes of vibration calculated for selected cluster sizes. Figure 8 shows these spectra and the corresponding density of vibrational states. All clusters, including the magic numbers Ca_{34}, Ca_{45}, Ca_{61}, and Ca_{82}, present a noticeable lack of vibrational modes with low frequencies. This gap becomes narrower as size increases. For Ca_{82}, the density of vibrational states at low frequencies is high enough to attempt a fit to a quadratic function of ν and extract an estimate of the Debye temperature. The result is $\Theta_D = 160$ K, which is 30% smaller than the bulk value of 230 K.

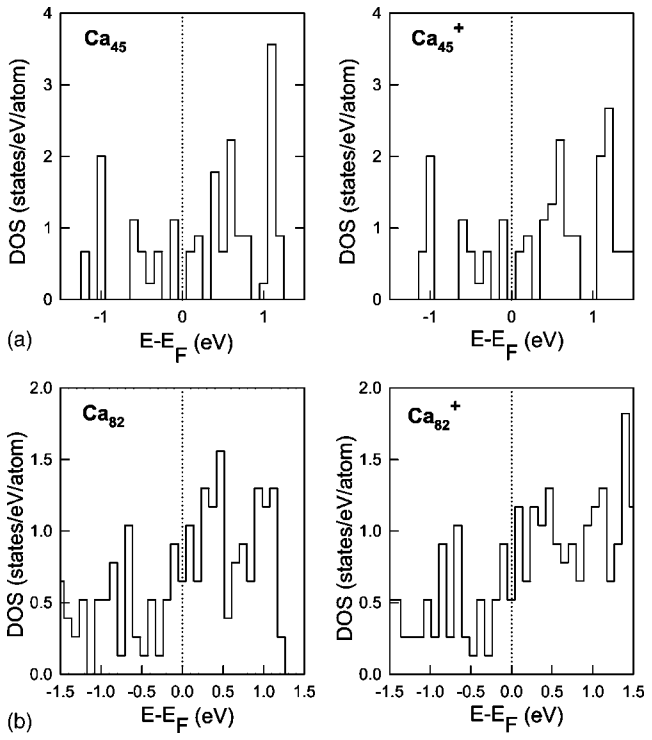

FIG. 7. Density of states around the Fermi energy at $T=0$. (a) Ca_{45} I_h and its cation; (b) Ca_{82} D_{3d} and its cation.

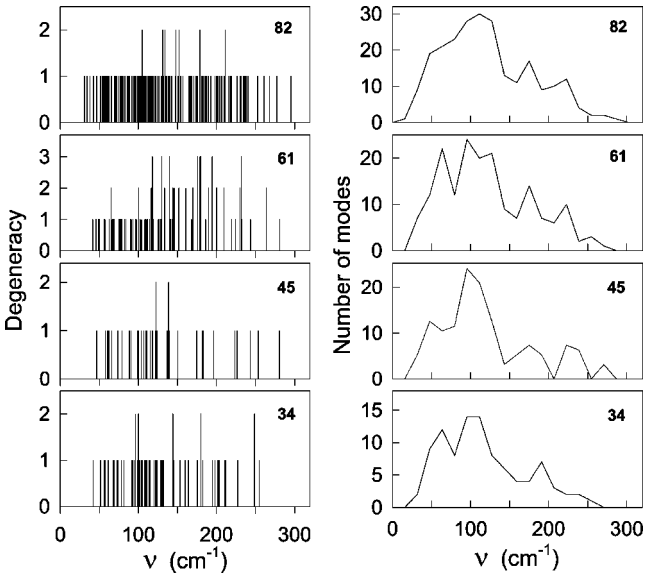

FIG. 8. Spectra of the normal mode vibrations and associated histogram for Ca_{34} D_{5h}, Ca_{45} I_h, Ca_{61} T_d, and Ca_{82} D_{3d}.

Once the vibrational frequencies are known, the standard harmonic quantum analysis of solids can be carried out to determine the Helmhotz free energy F. This vibrational-based thermodynamics is done in the canonical ensemble and addresses excitations of the quantum oscillators. Therefore, the "temperature" is that of a thermostat on an infinite number of identical systems, and not a result of time averaging the kinetic energy of the atoms in one isolated cluster. This quantum analysis was performed on the ground state of several structures, on both the magic number structures Ca_{34} D_{5h}, Ca_{45} I_h, Ca_{61} T_d, Ca_{82} D_{3d}, and on serveral other low-energy amorphouslike structures of these cluster sizes. The ground states of the amorphouslike isomers considered are 2.93, 1.37, 3.26, and 1.02 eV less stable than the ground state of the magic number structures. By analyzing the free-energy behavior as a function of temperature, we found that the amorphous isomers of these cluster sizes continue to be less stable than the very symmetric magic number structures up to temperatures of around 1200 K. We also investigated the relative stability of clusters around $N=82$ with respect to their neighbors by calculating the temperature dependence of the second difference of the free energy, $F(N+1)+F(N-1)-2F(N)$. The magic number $N=82$ in the D_{3d} symmetry persists even at temperatures of about 600 K. The zero point energy of the magic number structures 34, 45, 61, and 82 is 1.465, 2.060, 2.839, and 3.885 eV, respectively. The zero point energy of the amorphouslike structures is basically

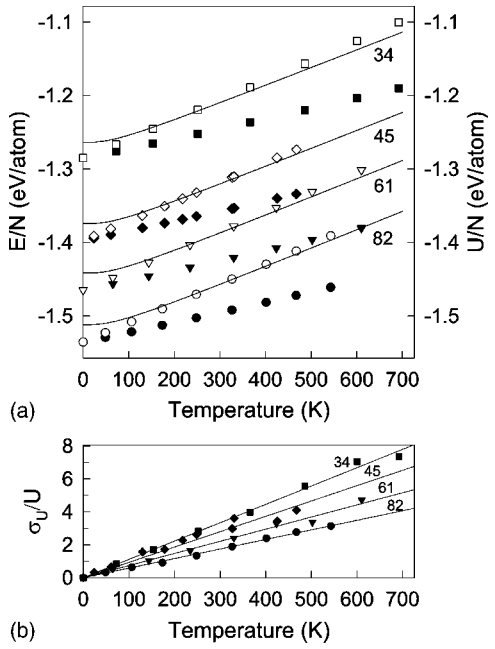

FIG. 9. (a) Internal energy per atom and potential energy per atom as a function of temperature for Ca_{34} D_{5h}, Ca_{45} I_h, Ca_{61} T_d, and Ca_{82} D_{3d}; (b) standard deviation of the potential energy as a function of temperature for the cluster sizes in (a).

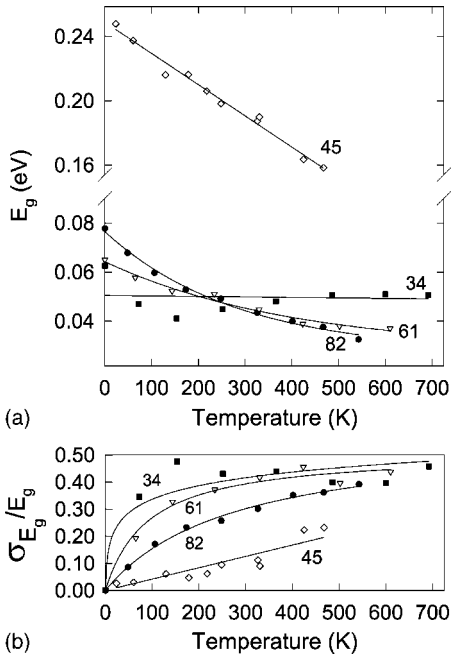

FIG. 10. (a) Energy gap of Ca_{34} D_{5h}, Ca_{45} I_h, Ca_{61} T_d, and Ca_{82} D_{3d}Ca as a function of temperature; (b) standard deviation of the energy gap as a function of temperature for the same nanoclusters.

identical to that of the symmetrical structures. For example, for Ca_{82} the lowest-energy amorphouslike structure has a binding energy of −1.523 eV/at and a zero point energy of 3.86 eV.

The harmonic analysis was also done to address the thermal stability of the calcium positive ions. For that, we performed the harmonic analysis on the ionized clusters around Ca_{82}^+ and calculated the second difference of the free energy as a function of temperature. At least within this TB approach, our results indicate insignificant changes due to the lack of one electron. At finite temperatures of about 600 K, both Ca_{82} and Ca_{82}^+ are relatively more stable than their size neighbors. This reconfirms that Ca_{82} D_{3d} is a predicted magic number from our calculation.

V. FINITE TEMPERATURE PROPERTIES OF Ca NANOCLUSTERS

Extensive TBMD at constant energy calculations were performed for selected cluster sizes. For every structure considered, the TBMD was run for 2000 time steps (of 1.5×10^{-15} sec each) to equilibrate, and averages reported in Figs. 9 and 10 were calculated over subsequent runs of 10 000 steps. These calculations are extremely cpu-intensive. For example, in the case of Ca_{82}, the cpu usage of a dedicated dual processor (Intel Xeon 3.08 GHz with hyper threading) is 11 s per MD step.

The cluster internal energy, $E(T)$, as a function of temperature increases linearly as shown in Fig. 9(a) for Ca_{34} D_{5h}, Ca_{45} I_h, Ca_{61} T_d, and Ca_{82} D_{3d} (empty symbols). Also shown in Fig. 9(a) are the averages of the potential energy $U(T)$ (black symbols). The continuous lines in this figure correspond to the internal energy calculated in the quantum harmonic approximation as described in the previous section. The agreement between the TBMD results and the harmonic results indicates that the harmonic approximation is indeed reliable up to temperatures of about 600 K. At very low temperatures, the zero point energy has a non-negligible contribution showing the quantum behavior of the material. Of course this effect is not captured by TBMD that only shows the classical contribution of atomic vibrations. The isometric specific heat can be easily calculated from $C_V = [dE(T)/dT]_{NV}$ giving the classical value of 3 per atom in units of k_B (Boltzmann's constant), for the four cluster sizes shown in Fig. 9(a). This is the expected result for solidlike clusters where the motion of the atoms is treated classically, as it is done by TBMD.

The electronic contribution to the specific heat is very small when compared to the dominant vibrational contribution. In fact, the Fermi temperature of Ca is 4.9×10^4 K. Therefore, the electronic contribution to $C_V/N/k_B$ at 600 K is only 0.05.

The fluctuations (standard deviation σ_U) of the potential energy $U(T)$ are illustrated in Fig. 9(b), showing that the magnitude of the potential-energy spread increases linearly with temperature and the expected decrease with system size $O(N^{-1/2})$ is visible. Furthermore, since all the TBMD calculations were done at constant energy, the fluctuations of the kinetic energy (or temperature) are equal to those of the potential energy.

There are no significant changes of the Fermi energy when temperature increases. On the other hand, for Ca_{61} and Ca_{82} the gap energies show a noticeable decrease with increasing temperature and display large fluctuations, as shown

in Figs. 10(a) and 10(b). However, Ca_{34} and Ca_{45} display a finite energy gap at all temperatures, with very large fluctuations. These fluctuations increase with temperature quite dramatically, pointing to the possibility of nanoclusters larger than $N=49$ transitioning to a metallic state at temperatures around 500 K. For example, at around 500 K, Ca_{82} displays a fluctuating energy gap of 0.04 ± 0.03 eV and a fluctuating DOS(E_F) of 0.11 ± 0.08 states/eV/at (about two electrons are promoted to virtual states). This is in contrast to the behavior of Ca_{45} at that temperature, where the energy gap is 0.16 ± 0.06 eV but the DOS(E_F) is zero. In the above values, the reported deviations pertain to twice the standard deviation.

In our TB calculations, as in other TB models, one is limited to searches of configuration space that exclude very short distances between any two atoms. This is related to the fitting strategy adopted. The purpose of including lattices at high densities in the TB fit was to allow for the possibility of atoms to approach up to a minimum distance of 2.9 Å. Therefore, bond lengths can squeeze to about 30%, at most. For this reason, we were unable to heat the larger clusters above temperatures of about 600 K (highest temperature in Fig. 9). It is apparent that when the cluster is metallic, the amplitudes of bond oscillations are large. In the case of Ca_{82}, the D_{3d} structure is still preserved at around 550 K, but amplitudes of vibration of several surface atoms are as large as 1.25 Å. If the system would be subject to higher temperatures (or pressures), this TB model would fail since it was not parametrized to study such conditions.

To study the thermal stability of the various structures, the atomic mean-squared displacement (MSD) was calculated with TBMD. For a cluster with N atoms, the averaged atomic MSD is defined by

$$\langle R^2\rangle = \frac{1}{M}\frac{1}{n_{\text{atoms}}}\sum_{s=1}^{M}\sum_{i=1}^{n_{\text{atoms}}}\langle[\mathbf{R}_i(t)-\mathbf{R}_i(t_{o_s})]^2\rangle, \qquad (5)$$

where $M=15$ is the number of initial time points t_{o_s}, n_{atoms} is either the number of core or surface atoms in a cluster with N atoms, $\mathbf{R}_i(t)$ is the position of the ith atom at time t, and the brackets refer to short time averages over 150 time steps. These short time averages were taken after the cluster was equilibrated at the desired temperature.

The averaged MSD behavior as a function of temperature is shown in Fig. 11 for cluster sizes 34, 45, 61, and 82. The error bars for each point correspond to twice the standard deviation. The clusters were in the energy basin of the zero-temperature structure at all temperatures within the range studied, and the structure was only deformed by the atomic vibrations. Open circles in this figure correspond to surface atoms MSDs, whereas the black circles illustrate the MSD of the inner core atoms. It is clearly seen that surface atoms have significantly larger displacements. An estimate of the melting temperature based on the Lindemann criterion[39] may be obtained when $MSD^{1/2}$ equals 15% of the average bond length. The horizontal lines in Fig. 11 correspond to average bond lengths (short-dashed line is for inner core, long-dashed line for surface). Combining the information in Figs. 5 and 11, it is apparent that the onset of surface premelting starts at around 700 K. However, by extrapolating results of the cluster core MSD, it is apparent that the cluster core melts at temperatures comparable to that of bulk calcium, which occurs at 1120 K. The premelting process should be understood as the amplitude of vibration of the surface atoms being significantly larger than those of the inner atoms, both types of atoms vibrating in the lowest-energy basin of the nanocluster. The TB model of bulk calcium[1] reproduced well the melting temperature of fcc calcium. The coefficient of thermal expansion was also obtained correctly. Therefore, calcium nanoclusters seem to begin the melting process by premelting of the surface at temperatures about 40% lower than the bulk. Based on the free-energy harmonic analysis described in the previous section, there is no structural transition up to 1200 K in either of these very symmetric clusters. Important to note is that Eq. (5) identifies the averaged mobility of the individual atoms with respect to a given configuration, as originally stated in Lindemann's criterion. Other authors have extended Lindemann's concept to changes in the averaged bond length[13] and have described premelting based on a classical analysis of the potential-energy landscape and on the thermal dependencies of the averaged bond length of structures associated to several minima in that landscape. In a TB calculation, that would be equivalent to accounting for several chemical isomerization reactions involving several electronic states. Depending upon the symmetry of such electronic states, some geometries can never be reached. This quantum signature seems to be absent in the Monte Carlo study of Ref. 13.

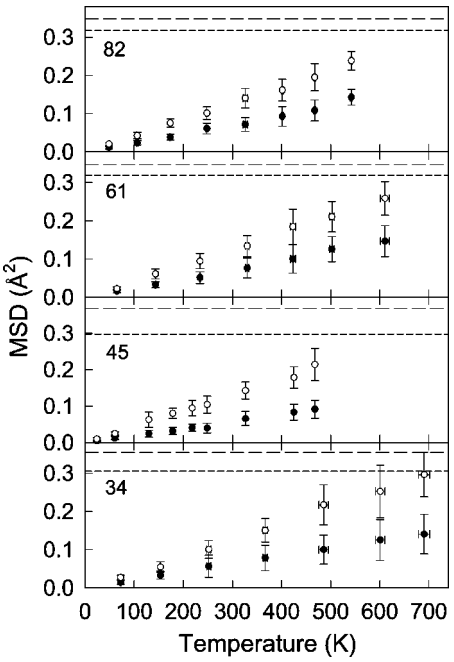

FIG. 11. Atomic mean-squared displacement as a function of temperature for Ca_{34} D_{5h}, Ca_{45} I_h, Ca_{61} T_d, and Ca_{82} D_{3d}. (a) Open circles are atoms in the cluster surface; (b) black circles are atoms in the cluster inner core. The long-dash and dashed lines correspond to 15% of the average bond distance in the surface and in the inner core, respectively.

VI. SUMMARY

For Ca nanoclusters with decades of atoms, a tight-binding model is constructed by incorporating the *ab initio* information of small Ca clusters and bulk calcium. Massive TBMD relaxations are carried out for nanoclusters measuring between 1 and 2 nm and containing 32 to 84 atoms to find the lowest-energy structure for each nanocluster. Magic numbers are found for clusters with 34, 37, 39, 45, 53, 57, 61, and 82 atoms. Three peculiar magic numbers, Ca_{34}, Ca_{37}, and Ca_{61}, were observed experimentally by Martin's group. The experimental magic number at $Ca_{80}-Ca_{81}$ was not found by this study. Instead we predict a strong magic number at 82. Several novel structures are predicted for clusters with the following sizes: 35, 38, 43, 50, 58, 59, 62, 63, and 76–84. Calcium clusters in this size range present incipient metallic behavior when they contain more than 49 atoms. Despite their metallic character, the structure of the magic numbers Ca_{61} and Ca_{82} is strikingly symmetric. These symmetric structures are very stable, and are not melted at temperatures of about 600 K. We predict that all clusters in the size range studied undergo a surface premelting that starts at about 700 K, but the inner-volumetric core of the cluster melts at temperatures comparable to the bulk material.

ACKNOWLEDGMENTS

E.B.B. acknowledges partial support from NSF Grants No. CTS-9806321 and No. DMS-9977373, ONR Grant No. N00014-98-1-0832, and the GMU Provost Office. Authors are very grateful to Dr. T. P. Martin for making available to them his unpublished experimental results, and to Dr. D. A. Papaconstantopoulos for informative discussions concerning the TB method.

*Electronic address: blaisten@gmu.edu

[1] G. M. Wang, D. A. Papaconstantopoulos, and E. Blaisten-Barojas, J. Phys. Chem. Solids **64**, 185 (2003).
[2] J. W. Mirick, C-H. Chien, and E. Blaisten-Barojas, Phys. Rev. A **63**, 023202 (2001).
[3] J. E. Hearn and R. L. Johnston, J. Chem. Phys. **107**, 4674 (1997).
[4] J. N. Murrell and R. E. Mottram, Mol. Phys. **69**, 571 (1990).
[5] T. P. Martin, U. Naher, T. Bergmann, H. Gohlich, and T. Lange, Chem. Phys. Lett. **183**, 119 (1991).
[6] T. P. Martin, Phys. Rep. **273**, 199 (1996).
[7] L. A. Heinebrődt, Ph.D thesis, Universitaät Stuttgart, Germany (1999).
[8] T. P. Martin (unpublished); see http://scs.gmu.edu/lcdm/Caspectrum.html.
[9] G. M. Wang, E. Blaisten-Barojas, A. E. Roitberg, and T. P. Martin, J. Chem. Phys. **115**, 3640 (2001).
[10] Y. Li, E. Blaisten-Barojas, and D. A. Papaconstantopoulos, Chem. Phys. Lett. **268**, 331 (1997).
[11] Y. Li, E. Blaisten-Barojas, and D. A. Papaconstantopoulos, Phys. Rev. B **57**, 15 519 (1998).
[12] C-H. Chien, E. Blaisten-Barojas, and M. R. Pederson, J. Chem. Phys. **112**, 2301 (2000).
[13] F. Calvo and F. Spiegelmann, J. Chem. Phys. **112**, 2888 (2000).
[14] M. J. Mehl and D. A. Papaconstantopoulos, Phys. Rev. B **54**, 4519 (1996).
[15] R. E. Cohen, M. J. Mehl, and D. A. Papaconstantopoulos, Phys. Rev. B **50**, 14 694 (1994).
[16] J. L. Mercer and M. Y. Chou, Phys. Rev. B **49**, 8506 (1994).
[17] M. S. Tang, C. Z. Wang, C. T. Chan, and K. M. Ho, Phys. Rev. B **53**, 979 (1996).
[18] H. Haas, C. Z. Wang, M. Fähnle, C. Elsässer, and K. M. Ho, Phys. Rev. B **57**, 1461 (1998).
[19] F. Liu, Phys. Rev. B **52**, 10 677 (1995).
[20] M. W. Finnis, A. T. Paxton, M. Methfessel, and M. van Schilfgaarde, Phys. Rev. Lett. **81**, 5149 (1998).
[21] S. Fabris, A. T. Paxton, and M. W. Finnis, Phys. Rev. B **61**, 6617 (2000).
[22] C. Barreteau, D. Spanjaard, and M. C. Desjonquéres, Phys. Rev. B **58**, 9721 (1998).
[23] C. Barreteau, R. Guirado-López, D. Spanjaard, M. C. Desjonquéres, and A. M. Oles, Phys. Rev. B **61**, 7781 (2000).
[24] P. Villaseñor-González, J. Dorantes-Dávila, H. Dreyssé, and G. M. Pastor, Phys. Rev. B **55**, 15 084 (1997).
[25] P. Alvarado, J. Dorantes-Dávila, and G. M. Pastor, Phys. Rev. B **58**, 12 216 (1998).
[26] M. Menon, J. Connolly, N. Lathiotakis, and A. Andriotis, Phys. Rev. B **50**, 8903 (1994).
[27] A. N. Andriotis and M. Menon, Phys. Rev. B **57**, 10 069 (1998).
[28] A. N. Andriotis and M. Menon, Phys. Rev. B **59**, 15 942 (1999).
[29] Y. Xie and J. A. Blackman, Phys. Rev. B **63**, 125105 (2001).
[30] R. Poteau and F. Spiegelmann, Phys. Rev. B **45**, 1878 (1991).
[31] J. C. Slater and G. F. Koster, Phys. Rev. **94**, 1498 (1954).
[32] G. M. Wang, Ph.D thesis, George Mason University, Fairfax, VA (2002).
[33] F. Kirchhoff, M. J. Mehl, N. I. Papanicolaou, D. A. Papaconstantopoulos, and F. S. Khan, Phys. Rev. B **63**, 195101 (2001).
[34] D. J. Wales and J. P. K. Doye, J. Phys. Chem. A **101**, 5111 (1997).
[35] J. P. K. Doye and D. J. Wales, J. Chem. Soc., Faraday Trans. **93**, 4233 (1997).
[36] J. P. K. Doye and D. J. Wales, New J. Chem. **22**, 733 (1998).
[37] E. Blaisten-Barojas, C-H. Chien, M. R. Pederson, and J. W. Mirick, Chem. Phys. Lett. **395**, 109 (2004).
[38] C. Kittel, *Introduction to Solid State Physics* (John Wiley & Sons Inc., New York, 1996).
[39] F. A. Lindemann, Phys. Z. **11**, 609 (1910).